# BUTANEDIOLS PRODUCTION FROM ERYTHRITOL ON RH PROMOTED CATALYST

E.M. VIRGILIO, C.L. PADRÓ† and M.E. SAD

*Catalysis Science and Engineering Research Group (GICIC)*
*Instituto de Investigaciones en Catálisis y Petroquímica -INCAPE-(UNL-CONICET)*
*CCT Santa Fe, Colectora RN 168 km 0, Paraje El Pozo, (3000) Santa Fe, Argentina.*
† *cpadro@fiq.unl.edu.ar*

***Abstract*— The C-O hydrogenolysis of Erythritol (ERY) to Butanediols was studied in aqueous solution at 473 K and 25 bar of $H_2$ using $Rh/ReO_x/TiO_2$ and the monometallic $Rh/TiO_2$ and $ReO_x/TiO_2$ catalysts. The solids were characterized by temperature programmed reduction (TPR), TEM and XPS. TPR and XPS showed that $ReO_x$ species are close to Rh particles leading to reduction at lower temperature than Re on monometallic catalyst. However, some segregated Rhenium species were suspected by TPR profile for the bimetallic catalyst and detected by TEM. $Re/TiO_2$ exhibited low activity forming only products from dehydration and epimerization. Although $Rh/TiO_2$ showed high activity (total conversion at 14 h), was more selective to C-C cleavage leading to lower carbon products. $Rh/ReO_x/TiO_2$, showed instead, a good activity and selectivity towards C-O hydrogenolysis route yielding 37.5% of Butanediols. Activation energy and reaction orders on ERY (0.58) and $H_2$ (0.53) were estimated from experiences made at different reaction conditions.**

***Keywords*— Butanediols – Erythritol - Hydrogenolysis – Rhodium catalysts**

## I. INTRODUCTION

Erythritol ($C_4H_{10}O_4$) is a promising C4 intermediate produced by fermentation of sugars (Moon *et al.*, 2010) that can be obtained from non-edible biomass derivatives. By C-O hydrogenolysis, valuable butanediols (BDOs) can be obtained but their consecutive C-O hydrogenolysis produces butanols and butane, while C-C cleavage leads to lower carbon products (C2-C3), which are less valuable compounds and therefore should be avoided. Butanediols, have many applications such as food flavorings, inks, perfumes, fumigants and production of resins. Polyol hydrogenolysis has been previously studied, particularly using glycerol as reactants in aqueous solution to produce 1,2-propanediol and 1,3-propanediol (Nakagawa *et al.*, 2010; Soares *et al.*, 2016). Typically, noble metal/support catalysts are used for hydrogenolysis reactions. Pt, Ru, Rh, and Ir have been investigated but Pt was less active, while Ru often promotes excessive C–C cleavage. To prevent the break of the carbon chain, an oxophilic promoter (Re, Mo or W) is added to the noble metal resulting in an improvement of the selectivity to the C-O hydrogenolysis (Chia *et al.*, 2011). The hydrogenolisis of glycerol on $Ir/ReO_x/SiO_2$ catalysts was previously studied (Nakagawa *et al.*, 2010) and it was suggested that diols are formed by the attack of hydrogen species, dissociated on $Ir^0$, to 1-glyceride species formed on the oxidized rhenium cluster. $Rh/MoO_x/SiO_2$ catalyst was also tested during 1,4- anhydroerythritol hydrogenolysis (Arai *et al.*, 2016) to 2-butanol. Other supports, more hydrothermally stable than $SiO_2$, such as $TiO_2$ or $ZrO_2$, were used to prepare $Rh/ReO_x$ bimetallic catalysts to promote the ERY hydrogenolysis to BDOs (Said *et al.*, 2017). The highest selectivity obtained to butanetriol and butanediol was 37% and 29% respectively, at 80% of ERY conversion (200°C, 120 bar $H_2$) when using 3.7wt%Rh-3.5wt.%$ReO_x/ZrO_2$. The effect of $H_2$ partial pressure on ERY initial rate was previously discussed while the effect of ERY initial concentration is still lacking.

Therefore, in this paper we focused on the C-O hydrogenolysis of ERY using $Rh/ReO_x/TiO_2$ in order to selectively produce BDO. We have compared the catalytic behavior of mono and bimetallic catalysts and estimated the reaction orders for ERY and $H_2$ as well as activation energy from kinetic experiments.

## II. EXPERIMENTAL SECTION

### A. Catalysts preparation

$TiO_2$ (Degussa P-25, 50 $m^2/g$, 85% anatase, 15% rutile) was used as catalysts support. Before impregnation, the $TiO_2$ was treated in air flow at 723 K for 4 h (heating rate 5 K/min). $Rh/TiO_2$ and $ReO_x/TiO_2$ catalysts were prepared by incipient wetness impregnation with an aqueous solution of $RhCl_3$ (Sigma-Aldrich, 99.9%) and $HReO_4$ (Sigma Aldrich, 99%) respectively. The bimetallic $Rh/ReO_x/TiO_2$ catalyst was prepared by impregnation of $Rh/TiO_2$ with $HReO_4$ aqueous solution. After impregnation, the catalysts were dried at 373 K for 24 h and treated in air at 723 K. The nominal Rh content was 1.8 wt% and rhenium content was determined in order to get Re/Rh molar ratio of 1.

### B. Catalysts characterization

Specific surface areas ($S_{BET}$) were measured by $N_2$ physisorption at 77 K in a Micromeritics Model ASAP 2020 apparatus. The crystalline structure of the samples were studied by X-ray diffraction (XRD) using a Shimadzu XD-D1 diffractometer and Ni-filtered CuKα monochromatic radiation for X-ray source. The metal content (Rh and Re) of the catalysts was determined by inductively coupled plasma atomic emission spectroscopy ICP-AES (Perkin Elmer, Optima 2100 DV).

Table 1. Catalysts characterization

| Catalysts | $S_{BET}$ ($m^2/g$) | TPR | XPS | | | | | |
|---|---|---|---|---|---|---|---|---|
| | | $H_2$ Uptake ($mol_{H2}\ g^{-1}h^{-1}$) | $(Re/Rh)_S$ | Rh 3d | | Re 4f | | |
| | | | | $Rh^{+3}$ | $Rh^0$ | $Re^{+7}$ | $Re^{+5}$ | $Re^{+4}$ |
| **$Rh/TiO_2$** | 48 | $2.1\cdot10^{-4}$ | - | 43% | 57% | - | - | - |
| **$ReO_x/TiO_2$** | 49 | $3.5\cdot10^{-4}$ | - | - | - | 20% | 80% | - |
| **$Rh/ReO_x/TiO_2$** | 49 | $5.3\cdot10^{-4}$ | 0.97 | 35% | 65% | - | 32% | 68% |

Temperature programmed reduction (TPR) was carried out in a fixed-bed reactor using $H_2$ (5%)/Ar (60 $cm^3$/min) and heating rate of 10 K/min from 298 K to 1073 K. $H_2$ (m/z=2) signal was analyzed by mass spectrometry in a Baltzers Omnistar unit. XPS analysis was performed on a Specs Multitechnical instrument equipped with a dual Al/Mg X-ray source and a PHOIBOS 150 hemispheric analyzer in fixed analyzer transmission mode (FAT). The spectra were obtained with step energy of 30 eV with Mg anode (200W). The pressure during the measurement was less than $1.10^{-9}$ mbar. Before the analysis, the samples were treated in 5% $H_2$/Ar flow during 0.5 h at 393 K and then evacuated in ultra-high vacuum for 2 h. Casa XPS (ver. 2.3.19) software was used to analyze Rh 3d and Re 4f peaks. Transmission electron microscope (TEM) images were acquired with JEOL 2100 plus. The samples were dispersed in ethanol using ultrasound and supported on Cu grids. More than 200 particles were measure to estimate the average particle size.

### C. Catalytic tests

Catalytic experiments were carried out in a batch reactor (Parr 4565). Prior the reaction, the catalyst was reduced ex-situ at 393 K (reduction temperature was chosen considering the maximum of the first peak during TPR experiments) for 1 h in $H_2$ flow (30 $cm^3$/min). After the reduction, the catalyst and erythritol aqueous solution (0.4 M) were loaded into the reactor and purged with $N_2$; then the reactor was heated up to reaction temperature (473 K) under stirring and finally, the desirable $H_2$ pressure was admitted (25 bar). Both liquid and gas phases were analyzed. Liquid samples were periodically collected and analyzed by HPLC (Shimadzu 20A) with refractive index detector (RID-20A) using a Bio-Rad Aminex HPX-87H ion exchange column with a flow rate of mobile phase ($H_2SO_4$ 5mM) of 0.6 mL/min. Gaseous products were quantified using an Agilent 6850 gas chromatograph equipped with a 30 m HP5 column (inner diameter: 0.32 mm, film thickness: 0.25 µm) and a flame ionization detector (FID). A gas chromatograph Thermo Scientific ISQ QD Simple Quadropole Mass Spectrometer with a 30 m TR-5MS column (inner diameter: 0.25 mm, film thickness: 0.25 µm) was used to identify some unknown products.

The conversion of erythritol was calculated as:

$$X_{ERY}^{t}(\%) = \frac{C_{ERY}^{0} - C_{ERY}^{t}}{C_{ERY}^{0}} \cdot 100 \qquad (1)$$

where $C_{ERY}{}^0$ is the initial ERY concentration and $C_{ERY}{}^t$ is the ERY concentration at a *t* time of the reaction.

The yield to *j* product ($\eta_j{}^t$) was calculated as:

$$\eta_j^t(\%) = \frac{C_j^t \cdot n_j^c}{C_{ERY}^0 \cdot n_{ERY}^c} \cdot 100 \qquad (2)$$

where $C_j^t$ is the concentration of j at a *t* time of the reaction and $n_j^c$ is the number of carbon of j.

## III. RESULTS AND DISCUSSION

### A. Catalysts characterization

Catalysts characterization results are presented in Table 1. The impregnations and thermal treatments did not significantly change the BET surface area of $TiO_2$. The $H_2$ consumption reported in Table 1 was calculated from the TPR profiles of mono and bimetallic catalysts. The $Rh/TiO_2$ TPR curve shows a broad peak center on 400 K, assigned to the complete reduction of $Rh^{+3}$ to $Rh^0$ as the $H_2$ uptake was similar to the theoretical value expected. The TPR for $Re/TiO_2$ catalyst has a narrow peak over 540 K accounting for the $H_2$ consumption for $Re^{+7}$ to $Re^0$ reduction in good agreement with results previously reported (Mitra *et al.*, 2001).The $Rh/ReO_x/TiO_2$ profile presented an asymmetric peak at about 400 K attributed at $Rh^{+3}$ reduction and rhenium species close to Rh particles that promotes its reduction, a second peak at higher temperatures was also detected related to the reduction of rhenium clusters far from Rh species. A $H_2$ consumption of $5.3\cdot10^{-4}$ $mol_{H2}$ $g^{-1}h^{-1}$ was calculated for bimetallic catalyst which is lower than the theoretical predicted ($8.7\cdot10^{-4}$ $mol_{H2}$ $g^{-1}h^{-1}$) and it is probably due to partial reduction of rhenium species. Actually, it was previously reported the stabilization of rhenium species at intermediate oxidation states in bimetallic catalysts (Koso *et al.*, 2011). Furthermore, a structure of Rh metal particles with attached $ReO_x$ clusters was suggested for these authors (Amada *et al.*, 2010).

X-ray photoelectron spectroscopy (XPS) was performed on the three catalysts reduced at 393 K. The Rh3d and Re4f spectra for $Rh/TiO_2$, $ReO_x/TiO_2$ and $Rh/ReO_x/TiO_2$ are displayed in Fig. 1. The relative abundance of each oxidation state of both Re and Rh species in the different materials are compiled in Table 1. The Rh3d profile of monometallic and bimetallic (Fig. 1 a and b, $Rh3d_{5/2}$ BE = 307eV) are similar with a significant proportion of $Rh^0$ (57% y 65%, respectively) in good agreement with Abe *et al.* (2001). On the contrary, the Re4f spectrum shows differences between $ReO_x/TiO_2$ and $Rh/ReO_x/TiO_2$ catalysts. The predominant rhenium species for monometallic catalysts was $Re^{+V}$ ($Re4f_{7/2}$ BE = 43.7eV), whereas the main oxidation state in the bimetallic solid was $Re^{+IV}$ ($Re4f_{7/2}$ BE = 42.4eV) (Cohen Sagiv *et al.*, 2013). The Re/Rh molar ratio estimated for bimetallic catalyst by XPS was 0.97.

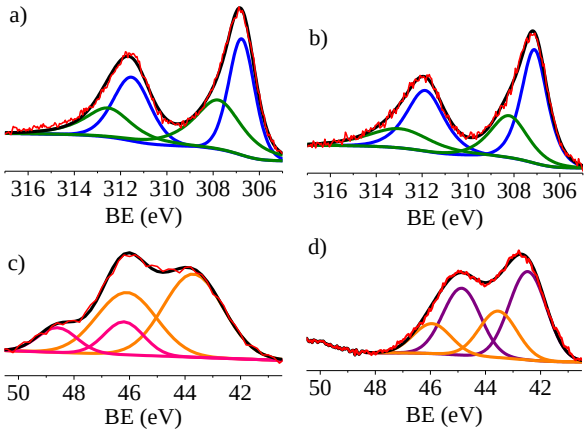


Figure 1: XPS spectra of monometallic and bimetallic catalysts of Rh 3d and Re 4f. a) $Rh/TiO_2$, b) $ReO_x/TiO_2$, c) and d) $Rh\text{-}ReO_x/TiO_2$. (—) $Rh^{+3}$, (—) $Rh^0$, (—) $Re^{+7}$, (—) $Re^{+5}$, (—) $Re^{+4}$, (—) Envelope, (—) Measure.

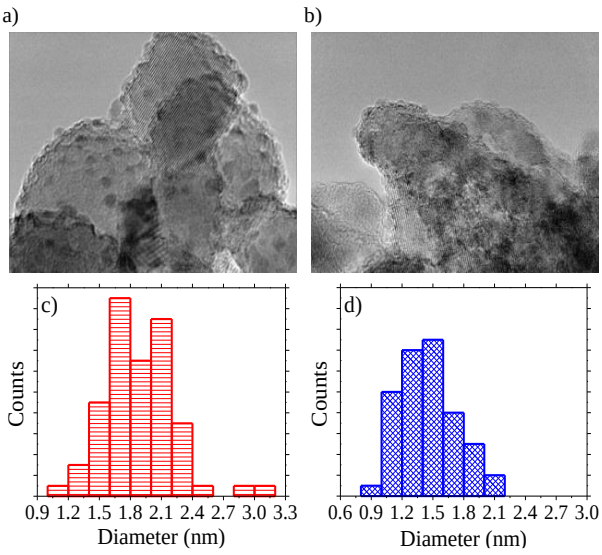


Figure 2: TEM images and particle size histogram of a) and c) $Rh/TiO_2$, b) and d) $Rh\text{-}ReO_x/TiO_2$

TEM images of $Rh/TiO_2$ and $Rh/ReO_x/TiO_2$ and the corresponding size histograms are shown in Fig. 2. Mean particle size was lower for the bimetallic catalyst (1.5 nm) than for the monometallic solid (1.8 nm), suggesting that the addition of rhenium oxide on $Rh/TiO_2$ slightly affects the particle size as previously reported (Said *et al.*, 2017). Energy-dispersive X-ray spectroscopy (EDS) was performed over several randomly selected images of $Rh/ReO_x/TiO_2$ and we have estimated an average Re/Rh atomic ratio of 0.9 with a few areas with higher Re content (Re/Rh ratio up to 1.25 as depicted in Fig. 3).

**B. Catalytic results**

Erythritol (ERY) can react in the presence of $H_2$ on $Rh/ReO_x$/support to form several products as shown in Fig 4. The main routes are: *i)* dehydration to form mainly 1,4 anhydroerythritol (14AE), 3-hydroxytetrahydrofuran (3OTHF) and tetrahydrofuran(THF), *ii)* C-C cleavage to render C2+C3 products such as ethylene glycol (EG) and glycerol (GLY), *iii)* C-O cleavage to form butanetriols (BTO), butanediols (BDO) and butanols (BuOH) and *iv)* epimerization to threitol. The desired reaction path to BDOs formation, the C-O hydrogenolysis of erythritol, produces 1,2,3-butanetriol and 1,2,4-butanetriol and subsequent C-O cleavage of these products can form the four butanediols isomers (1,2BDO, 2,3BDO, 1,4BDO and 1,3BDO). However, further C-O cleavage leads to lower value products: butanols and butane.

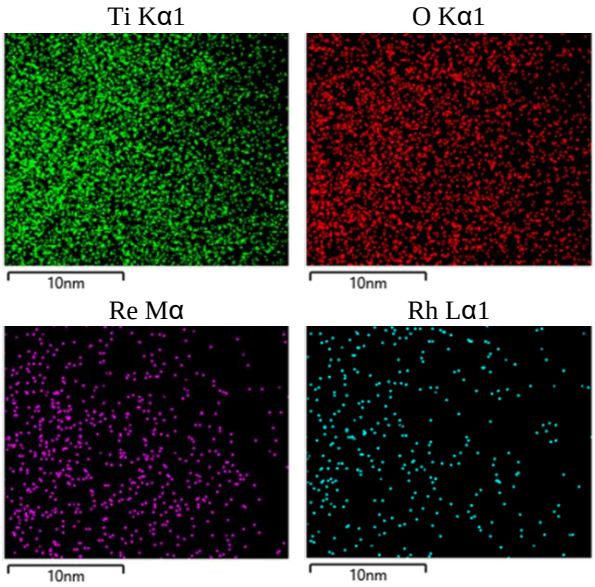


Figure 3: Dark Field images with EDS analysis

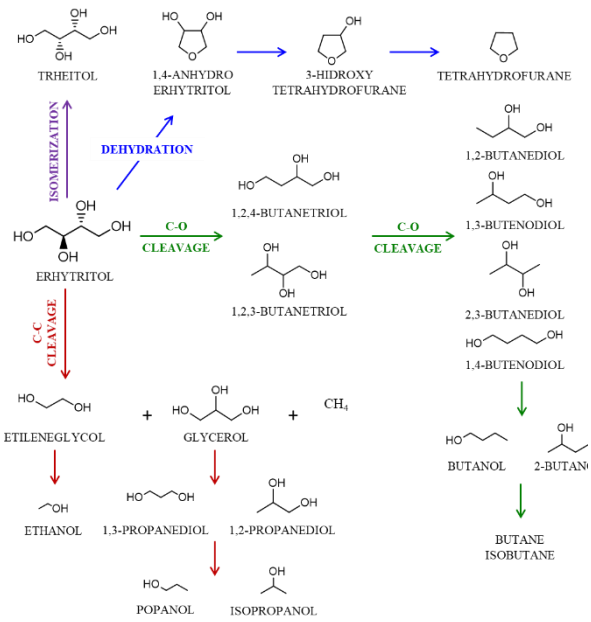


Figure 4: Reaction network for erythritol conversion

Preliminary reactions without catalysts or using only the support ($TiO_2$) were conducted at standard reaction conditions (473 K, 25 bar $H_2$, $C^0_{ERY}$=0.4 M). Erythritol conversion was null without any catalyst after 6 h of reaction while a 6 % conversion was reached when using $TiO_2$ (catalyst concentration=0.0125 g $mL^{-1}$); the only product formed was 1,4AE and no gaseous pro-

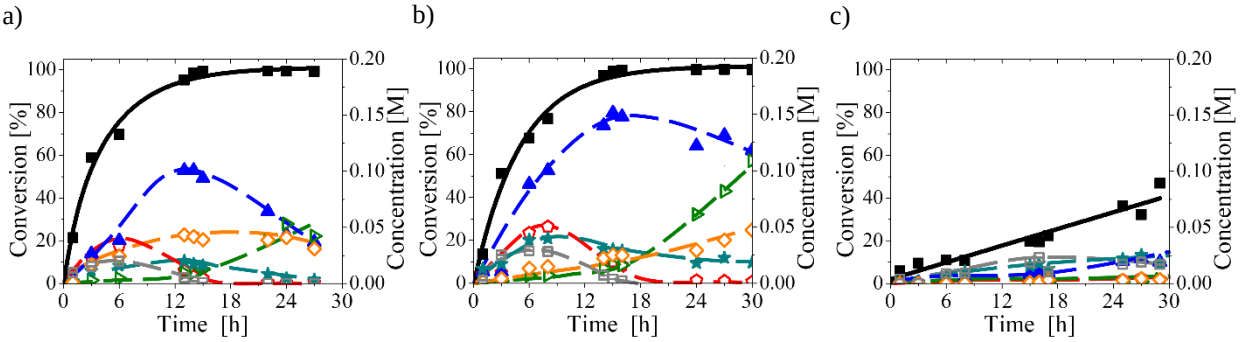


Figure 5: Evolution of the concentrations of ERY and products as a function of time. (■) ERY, (⬠) BTOs, (▲) BDOs, (▷) BuOHs, (★) Cyclic, (◇) $C_3$+$C_2$, (▭) TRE. a) $Rh/TiO_2$, b) $Rh\text{-}ReO_x/TiO_2$, c) $Re/TiO_2$ [0.4 M ERY, 473 K, 25bar $H_2$, 12.5 $g_{catalyst}$ $L^{-1}$]

ducts were detected. Additional catalytic tests were performed to ensure the absence of diffusional limitations.

Figure 5 shows the evolution of ERY conversion and product concentrations as function of reaction time using $Rh/TiO_2$ (a), $Rh/ReO_x/TiO_2$ (b) and $ReO_x/TiO_2$ (c) at standard conditions. $ReO_x/TiO_2$ exhibited very low activity reaching 40% conversion after 28 h of reaction.

Main products formed on this catalyst come from the dehydration (cyclic) and epimerization (threitol) of ERY, both reactions can be catalyzed by Lewis acid sites as the sites present on $ReO_x$ and also on $TiO_2$. In fact, it was observed in the literature that the presence of $ReO_x$ species enhanced the isomerization of allylic alcohols (Morrill and Grubbs, 2005). The addition of noble metal resulted in more active catalysts ($Rh/TiO_2$ and $Rh/ReO_x/TiO_2$) reaching total ERY conversion before 16 h of reaction. Product evolution was qualitatively similar on both catalysts. Butanetriols were formed from the beginning of reaction; the BTO concentration curve first increases, reaches a maximum and then decreases. This tendency is in good agreement with their role as primary products that directly are formed from reactant and then undergo further C-O hydrogenolysis to form BDO. However it is worth to note that the maximum concentration of BTO was higher on bimetallic catalyst ($C_{BTO}$=0.03 M at 6 h on $Rh/TiO_2$; $C_{BTO}$=0.05 M at 8 h on $Rh/ReO_x/TiO_2$). Butanediols were the main products formed most of the reaction time on both catalysts. Similarly to BTO curve, the BDO curve presents a maximum and then decreases due to butanols/butanes formation. As observed with BTO curve, the maximum concentration of BDO reached a value greater on $Rh/ReO_x/TiO_2$ (0.15 M) than observed on $Rh/TiO_2$ (0.1 M). Note that these values correspond to a yield of 37.5% and 25% respectively. Butanols concentration curve displays an inflection point at 14 h and monotonically increases during 30 h reaction. Butanes were actually detected in gas phase after 30 h in low concentrations; for example, about 10% of the erythritol reacted after 30 h reaction on $Rh/ReO_x/TiO_2$ was converted into gaseous products (mostly butane and methane). Threitol and cyclic products (principally14AE) were formed by isomerization and dehydration directly from erythritol, and also reach a maximum. In the case of 14AE, the subsequent decrease in the yield is related to the THF formation by consecutive reaction as detected in the gas phase after 30 h. Since threitol is much less reactive than Erythritol (Said *et al.*, 2017), the diminution of its concentration can be associated to its further transformation into erythritol caused by the high consume of reactant after the first 8 h reaction. Finally, the formation of products from C-C scission (C2+C3) increases with time, however on the monometallic catalyst goes through a maximum probably due to further C-C cleavage leading to light products that go to gas phase. Some conclusion can be drawn from these results: i) the presence of noble metal is required to activate the $H_2$ and produce the C-O and C-C hydrogenolysis; ii) $ReO_x$ species deposited on Rh decreased the C-C scission and promote the C-O hydrogenolysis forming selectively the desired products (BDO) reaching a 37.5% yield at 14 h of reaction. The highest BDO yield previously reported in literature was 23.3% using Rh-based catalyst and similar reaction conditions (Said *et al.*, 2017). From these results and previous papers (Nakagawa et al. 2010), it can be suggested that butanediols are formed from the attack of $H_2$ activated on Rh metal to the ERY adsorbed on $ReO_x$ clusters.

In order to study the influence of temperature, erythritol concentration, and $H_2$ pressure on the reaction rate, experiments were carried out at different conditions (Table 2) using $Rh/ReO_x/TiO_2$ (catalyst concentration=12.5 $g_{catalyst}$ $L^{-1}$). Initial reaction rate of ERY conversion were determined from the slope at t=0 of the ERY concentration vs time curve for each experiment and the values obtained are included in Table 2. The initial rate increases as expected with an increment in temperature, but also with the ERY concentration and $H_2$ pressure evidencing a positive order on both reactants. We proposed a simple expression for the reaction rate (Eq. 3) with the aim to estimate the reaction orders.

$$r^0_{ERY} = k \cdot {C^0_{ERY}}^{\alpha} \cdot {P_{H2}}^{\beta} \qquad (3)$$

In Fig. 6, the logarithm of initial rate ($r^0_{ERY}$) was plotted as a function of the logarithm of ERY concentration and $H_2$ pressure (a) and versus 1/T (b). From these graphs the order on both reactants as well as the activa-

Table 2. Catalytic results for ERY hydrogenolysis on $Rh/ReO_x/TiO_2$

| En-try | $C^0_{ERY}$ (M) | $P_{H2}$ (bar) | Temp. (K) | $r^0_{ERY}$ $\left(\frac{mmol\ ERY}{g_{Rh}\cdot h}\right)$ |
|---|---|---|---|---|
| 1 | 0.4 | 25 | 423 | 272 |
| 2 | 0.4 | 25 | 448 | 384 |
| 3 | 0.4 | 25 | 473 | 584 |
| 4 | 0.4 | 25 | 498 | 699 |
| 5 | 0.2 | 25 | 473 | 443 |
| 6 | 0.6 | 25 | 473 | 816 |
| 7 | 0.4 | 15 | 473 | 576 |
| 8 | 0.4 | 35 | 473 | 901 |

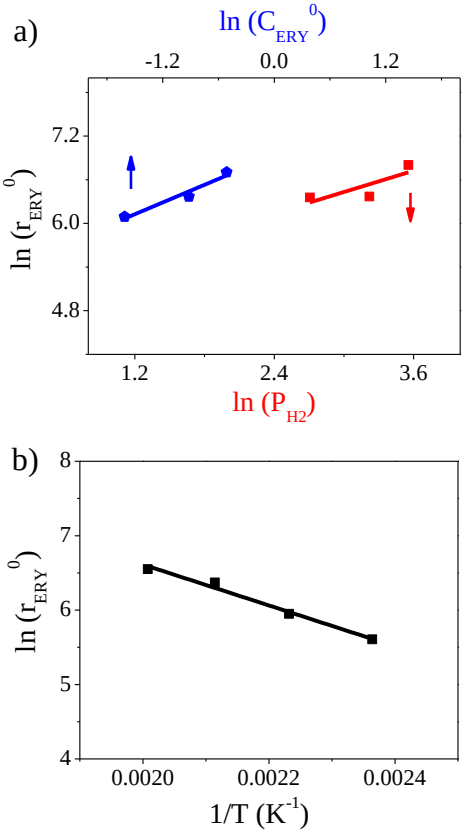


Figure 6: a) (■) ln ($r^0_{ERY}$) vs ln ($P_{H2}$), (⬟)ln ($r^0_{ERY}$) vs ln ($C_{ERY}{}^0$), b) (■)ln ($r^0_{ERY}$) vs 1/T

tion energy can be calculated, giving a value of α=0.58 (reaction order for ERY concentration) and β=0.53 (reaction order for $H_2$ pressure). Activation energy calculated from Fig. 6b was 26.6 KJ/mol, similarly to other values for C-O hydrogenolysis of polyols previously reported in literature (Sciences, 2004). The positive reaction order lower than 1 for erythritol can be interpreted by the strong adsorption of this reactant on $ReO_x$ species of $Rh/ReO_x/TiO_2$ whereas the reaction order close to 0.5 for $H_2$ pressure is in good agreement with its dissociative adsorption on $Rh^0$. Others authors have reported reaction orders about 0.5 for polyol concentrations during hydrogenolysis reactions; for example an order of 0.5 and 0.7 with respect to the substrate concentration was estimated for hydrogenolysis of 3-HTHF on $Ir/ReO_x/SiO_2$ and $Rh/ReO_x/SiO_2$, respectively (Chen *et al.*, 2012) and 0.6 for hydrogenolysis of 1,4AE on

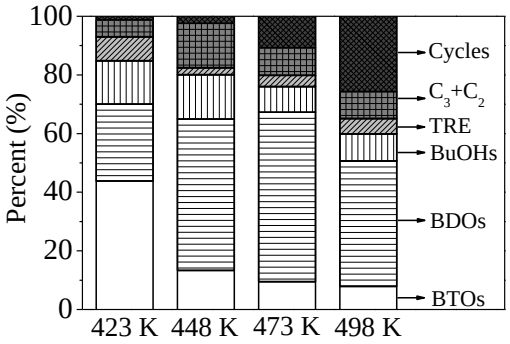


Figure 7: Products distribution at different temperatures over $Rh/ReO_x/TiO_2$ catalyst at maximum yield to butanediols. [0.4 M ERY, 25bar $H_2$, 12.5 $g_{catalyst}L^{-1}$]

$Rh/MoO_x/SiO_2$ (Arai *et al.*, 2016). Regarding the order determined for $H_2$ pressure some discrepancies are found in literature. Some authors have estimated an order of 0.85 when using $Ir/ReO_x/SiO_2$ (Amada *et al.*, 2012) while others have found positive order although close to zero on $Rh/ReO_x/TiO_2$ but close to 1 on $Rh/ReO_x/ZrO_2$ (Said *et al.*, 2017).

Moreover, the product distribution calculated at the time that the curve of BDO reaches the maximum for all temperatures employed are plotted in Fig. 7. BTO concentration decreases at high temperature, meanwhile BDO goes through a maximum at 473 K. As the temperature increases, the product from dehydration (mainly 1,4AE) significantly increases, demonstrating that this reaction path is highly affected by the temperature (high activation energy) as previously informed (Said *et al.*, 2017).

## IV. CONCLUSIONS

$Rh/ReO_x/TiO_2$ and the monometallic $Rh/TiO_2$ and $Re/TiO_2$ were prepared and characterized. From results of TPR and XPS, it can be deduced that most of $ReO_x$ species are close to Rh particles in bimetallic catalyst leading to reduction at lower temperature than rhenium on monometallic catalyst. However, some segregated rhenium species were detected both by TPR and TEM. Furthermore, $ReO_x$ stabilized on low oxidation state but no complete reduction is achieved.

The C-O hydrogenolysis of Erythritol to valuable products like butanediols was efficiently catalyzed by $Rh/ReO_x/TiO_2$ allowing to obtain a BDO yield higher than previously reported (37.5%). Kinetic of the reaction was studied by performing experiments at different reaction conditions. Activation energy of 26.6 KJ/mol and reaction orders on ERY and $H_2$ close to 0.5 were estimated indicating a probably strong adsorption of ERY on $ReO_x$ species and $H_2$ on metallic Rh particles.

## ACKNOWLEDGEMENTS

We thank the Universidad Nacional del Litoral (UNL), the Agencia Nacional de Promoción Científica y Tecnológica (ANPCyT) and CONICET, Argentina, for the

financial support of this work. We also thank ANPCyT for the purchase of the SPECS multitechnique analysis instrument (PME8-2003).

## REFERENCES

Abe, Y, Kato, K., Kawamura, M. and Sasaki, K. (2001). "Rhodium and Rhodium Oxide Thin Films Characterized by XPS Rhodium and Rhodium Oxide Thin Films Characterized by XPS," *Surface Science Spectra*, **8**, 117–125.

Amada, Y, Koso, S., Nakagawa, Y. and Tomishige, K. (2010). "Hydrogenolysis of 1,2-Propanediol for the Production of Biopropanols from Glycerol," *ChemSusChem*, **3**, 728–736.

Amada, Y., Watanabe, H., Hirai, Y., Kajikawa, Y., Nakagawa, Y. and Tomishige, K. (2012). "Production of biobutanediols by the hydrogenolysis of erythritol," *ChemSusChem*, **5**, 1991–1999.

Arai, T., Tamura, M., Nakagawa, Y. and Tomishige, K. (2016). "Synthesis of 2-Butanol by Selective Hydrogenolysis of 1,4-Anhydroerythritol over Molybdenum Oxide-Modified Rhodium-Supported Silica," *ChemSusChem*, **9**, 1680–1688.

Chen, K., Moria, K., Watanabe, H., Nakagawa, Y., Tomishige, K. (2012). "C–O bond hydrogenolysis of cyclic ethers with OH groups over rhenium-modified supported iridium catalysts," *Journal of Catalysis*, **294**, 171-183.

Chia, M., Pagán-Torres, Y., Hibbitts, D., Tan, Q., Pham, H.N., Datye, A.K., Neurock, M., Davis, R.J. and Dumesic, J.A. (2011). "Selective hydrogenolysis of polyols and cyclic ethers over bifunctional surface sites on rhodium-rhenium catalysts," *Journal of the American Chemical Society*, **133**, 12675–12689.

Cohen Sagiv, M., Eliaz, N. and Gileadi, E. (2013). "Incorporation of iridium into electrodeposited rhenium-nickel alloys," *Electrochimica Acta*, **88**, 240–250.

Koso, S., Nakagawa, Y. and Tomishige, K. (2011). "Mechanism of the hydrogenolysis of ethers over silica-supported rhodium catalyst modified with rhenium oxide," *Journal of Catalysis*, **280**, 221-229.

Mitra, B., Gao, X., Wachs, I.E., Hirt, A.M. and Deo, G. (2001). "Characterization of supported rhenium oxide catalysts: Effect of loading, support and additives," *Physical Chemistry Chemical Physics*, **3**, 1144–1152.

Moon, H.J., Jeya, M., Kim, I.W. and Lee, J.K. (2001). "Biotechnological production of erythritol and its applications," *Applied Microbiology and Biotechnology*, **86**, 1017–1025.

Morrill, C. and Grubbs, R.H. (2005). "Highly Selective 1,3-Isomerization of Allylic Alcohols via Rhenium Oxo Catalysis," *J.Am.Chem.Soc.*, **127,** 2842-2843.

Nakagawa, Y., Shinmi, Y., Koso, S., Tomishige, K. (2010). "Direct hydrogenolysis of glycerol into 1,3-propanediol over rhenium-modified iridium catalyst," *Journal of Catalysis*, **272**, 191–194.

Said, A., Da Silva Perez, D., Perret, N., Pinel, C. and Besson, M. (2017). "Selective C−O Hydrogeno-lysis of Erythritol over Supported Rh-ReOxCatalysts in the Aqueous Phase," *ChemCatChem*, **9**, 2768–2783.

Sciences, N. (2004). "Correlation between preexponential and activation energy of Isoamylalcohol hydrogenolysis on Platinum catalysts," *Indonesian Journal of Chemistry*, **4**, 1–5.

Soares, A.V.H., Salazar, J.B., Falcone, D.D., Vasconcellos, F.A., Davis, R.J. and Passos, F.B. (2016). "Chemical A study of glycerol hydrogenolysis over Ru–Cu/Al2O3 and Ru–Cu /ZrO2 catalysts," *Journal of Molecular Catalysis A*, **415**, 27–36.

**Received October 21, 2019**
**Sent to Subject Editor October 22, 2019**
**Accepted January 2, 2020**
**Recommended by Guest Editor: J. Isabel Di Cosimo**